Relationships between Large-Scale Regime Transitions and Major Cool-Season Precipitation Events in the Northeastern United States

HEATHER M. ARCHAMBAULT, DANIEL KEYSER, AND LANCE F. BOSART

Department of Atmospheric and Environmental Sciences, University at Albany, State University of New York, Albany, New York

(Manuscript received 29 January 2010, in final form 5 April 2010)

ABSTRACT

This observational study investigates statistical and synoptic–dynamic relationships between regime transitions, defined as a North Atlantic Oscillation (NAO) or Pacific–North American pattern (PNA) index change from at least a 1 standard deviation anomaly to at least a 1 standard deviation anomaly of opposite sign within 7 days, and cool-season (November–April) northeastern U.S. (NE) precipitation. A statistical analysis is performed of daily cool-season NE precipitation during all NAO and PNA transitions for 1948–2003, and a composite analysis and case study of a major cool-season NE precipitation event occurring during a positive-to-negative NAO transition are conducted. Datasets used are the 0.25° NCEP Unified Precipitation Dataset, the 2.5° NCEP–NCAR reanalysis, and the 1.125° 40-yr ECMWF Re-Analysis (ERA-40).

Results of the statistical analysis suggest that cool-season NE precipitation tends to be enhanced during positive-to-negative NAO and negative-to-positive PNA transitions, and suppressed during negative-to-positive NAO and positive-to-negative PNA transitions. Of the four types of regime transitions, only the positive-to-negative NAO transition is associated with substantially more frequent major cool-season NE precipitation events compared to climatology. Results of the composite analysis and case study indicate that a surface cyclone and cyclonic wave breaking associated with the major NE precipitation event can help produce a high-latitude blocking pattern over the North Atlantic characteristic of a negative NAO pattern via thermal advection, potential vorticity transport, and diabatic processes.

1. Introduction

The character of the large-scale flow can significantly influence midlatitude precipitation patterns. The North Atlantic Oscillation (NAO; e.g., Walker and Bliss 1932; Wallace and Gutzler 1981; Barnston and Livezey 1987; Feldstein 2003; Benedict et al. 2004; Rivière and Orlanski 2007) and the Pacific–North American pattern (PNA; e.g., Wallace and Gutzler 1981; Barnston and Livezey 1987; Feldstein 2002), the predominant modes of NH low-frequency atmospheric variability, substantially modulate the amount of precipitation received by Europe and central North America, respectively. While the relationship is more subtle, these low-frequency modes also affect precipitation in the northeastern United States (NE; e.g., Leathers et al. 1991; Hurrell 1995; Coleman and Rogers 2003; Notaro et al. 2006; Archambault et al. 2008). The NAO and PNA affect cool-season NE precipitation because the NAO and PNA phases are linked to the strength and location of the jet stream and storm track associated with these respective modes.

The NAO is defined as a north–south dipole of upper-tropospheric geopotential height or sea level pressure (SLP) anomalies over the mid- and high-latitude North Atlantic (e.g., Wallace and Gutzler 1981; Hurrell 1995). The positive NAO (NAO^+) phase is characterized by a relatively strong Icelandic low and Azores high and is manifested as an anomalously strong, southwest–northeast-oriented jet stream and storm track extending from near the NE coast to northern Europe. Conversely, a negative NAO (NAO^-) phase, with its relatively weak Icelandic low and Azores high, is manifested as an anomalously weak, west–east-oriented jet stream and storm track extending from the Mid-Atlantic coast to central Europe (e.g., Lau 1988; Rogers 1990). Recent studies (e.g., Shabbar et al. 2001; Benedict et al. 2004; Croci-Maspoli et al. 2007; Luo et al. 2007a,b; Woollings

Corresponding author address: Heather M. Archambault, Department of Atmospheric and Environmental Sciences, University at Albany, State University of New York, ES-234, 1400 Washington Ave., Albany, NY 12222.
E-mail: heathera@atmos.albany.edu

DOI: 10.1175/2010MWR3362.1

et al. 2008) have noted a link between the NAO^- phase and a greatly increased frequency of blocking (e.g., Rex 1950a,b; Pelly and Hoskins 2003a; Berrisford et al. 2007) in the high-latitude North Atlantic, and it has been suggested that the NAO^- phase and high-latitude North Atlantic blocking are manifestations of the same phenomenon (Luo et al. 2007a,b; Woollings et al. 2008).

The PNA is defined as four upper-tropospheric geopotential height or SLP anomalies of alternating sign that collectively resemble a stationary Rossby wave train arcing along an approximate great circle path from the east-central tropical Pacific to the southeastern United States (e.g., Wallace and Gutzler 1981; Barnston and Livezey 1987). The positive PNA (PNA^+) phase is characterized by an amplified ridge–trough pattern over North America, which translates to a jet stream and storm track that are displaced farther equatorward than usual over the eastern United States. Conversely, a negative PNA (PNA^-) phase is characterized by a less amplified trough–ridge pattern over North America, with a jet stream and storm track that are displaced farther poleward than usual over the eastern United States (e.g., Leathers et al. 1991).

The close proximity of the jet stream and storm track to the NE during NAO^+ and PNA^- phases, and their more remote positions during NAO^- and PNA^+ phases, are concordant with findings that the NE is prone to relatively wet (dry) conditions during NAO^+ and PNA^- (NAO^- and PNA^+) phases (e.g., Notaro et al. 2006; Archambault et al. 2008). Archambault et al. (2008) noted that cool-season (November–April) NE precipitation during 1948–2003 tends to be above normal during PNA^- regimes[1] because of the increased likelihood of light and moderate precipitation events. Conversely, they noted that cool-season NE precipitation tends to be below normal during PNA^+ regimes because of the decreased likelihood of light and moderate precipitation events. Archambault et al. (2008) also found that cool-season NE precipitation tends to be above normal during NAO^+ regimes and below normal during NAO^- regimes, although these relationships were not found to be statistically significant. Finally, they showed that none of these four large-scale regimes is associated with an increased likelihood of major cool-season NE precipitation events. The foregoing results are broadly consistent with other research indicating that monthly cool-season NE precipitation is moderately correlated with the NAO phase (Hurrell 1995; Dai et al. 1997; Notaro et al. 2006) and moderately anticorrelated with the PNA phase (Leathers et al. 1991; Notaro et al. 2006).

Although previous research has not found relationships between NAO and PNA phases and major cool-season NE precipitation events, it is speculated that relationships may exist between NAO and PNA phase changes and major cool-season NE precipitation events. This speculation follows from the recognition that major cool-season NE precipitation events occur primarily in conjunction with synoptic-scale extratropical cyclones (e.g., Sisson and Gyakum 2004; Archambault et al. 2008), and that synoptic-scale transient disturbances, which include extratropical cyclones, are known to contribute to large-scale flow reconfigurations through transports of vorticity, potential vorticity (PV), heat, and momentum. Synoptic-scale transient disturbances have been shown to contribute to large-scale flow reconfigurations such as the establishment of the phases of the NAO (e.g., Benedict et al. 2004; Franzke et al. 2004; Löptien and Ruprecht 2005; Rivière and Orlanski 2007; Woollings et al. 2008) and PNA (e.g., Feldstein 2002; Orlanski 2005; Croci-Maspoli et al. 2007), the onset of blocking (e.g., Sanders and Gyakum 1980; Shutts 1983, 1986; Colucci 1985, 1987; Mullen 1986; Pelly and Hoskins 2003a; Berrisford et al. 2007), and the development of persistent large-scale positive and negative geopotential height anomalies (e.g., Dole and Gordon 1983; Dole 1986a,b; Dole and Black 1990; Black and Dole 1993; Higgins and Schubert 1994; Dole 2008, sections 3a and 3b). To the extent that NAO and PNA phase changes correspond to large-scale flow reconfigurations that are associated with synoptic-scale extratropical cyclones, and given that extratropical cyclones are associated with cool-season precipitation, the possibility exists that NAO and PNA phase changes are related to major cool-season NE precipitation events. Accordingly, the purpose of this paper is to investigate relationships between NAO and PNA phase changes on synoptic time scales (i.e., regime transitions) and major cool-season NE precipitation events.

In recent years, the behavior of the NAO and PNA has become predictable by global forecast models as much as two weeks in advance during the cool season. It has been noted by Johansson (2007) that global forecast models exhibit greater skill in predicting the NAO and PNA than the overall NH extratropical flow pattern, and may be particularly skillful in predicting extreme phases of the NAO and PNA. Thus, quantifying relationships between NAO and PNA regime transitions and major cool-season NE precipitation events may help improve medium-range NE precipitation forecasts by providing forecasters with advance notice of the possible occurrence of major precipitation events.

[1] Archambault et al. (2008) defined regimes as periods when the NAO or PNA index exceeds ±1.0 standard deviations (SDs) for at least 7 days.

TABLE 1. The number of cool-season regime transitions identified, total number of days falling in each regime transition category, and duration of regime transitions.

Regime transition	No. of regime transitions	Total No. of days	Duration of transition (days)	
			Mean	SD
NAO^+ to NAO^-	42	225	5.4	1.2
NAO^- to NAO^+	59	331	5.6	1.1
PNA^+ to PNA^-	61	338	5.5	1.1
PNA^- to PNA^+	65	350	5.4	1.1

The paper is organized as follows. A statistical analysis of daily cool-season NE precipitation during all objectively identified NAO and PNA regime transitions for 1948–2003 is presented in section 2. The statistical analysis motivates a composite analysis of 11 major cool-season NE precipitation events that occur during a NAO^+ to NAO^- transition, which is documented in section 3. A case study of the 29–30 November 1963 NE heavy rainstorm, one of the events included in the composite, is detailed in section 4. The results of this study are discussed in section 5, and a summary and conclusion follow in section 6.

2. Statistical analysis

a. Methodology and data

Cool-season large-scale regime transitions are objectively identified using daily standardized NAO and PNA indices. The daily standardized NAO and PNA index time series are constructed from 2.5° × 2.5° gridded National Centers for Environmental Prediction–National Center for Atmospheric Research (NCEP–NCAR) reanalysis (Kalnay et al. 1996; Kistler et al. 2001) 500-hPa geopotential height data for 1948–2003 following Archambault et al. (2008, see their section 2a). A regime transition is defined as when the phase of the daily NAO or PNA changes from a 1 standard deviation (SD) anomaly (i.e., an index of at least ±1.0) to a 1 SD anomaly of the opposite sign within 7 days. This definition is chosen in order to examine extreme regime transitions on a synoptic time scale while retaining an adequate sample size for statistical analysis. Information about the number of cool-season regime transitions identified, the total number of days falling within the regime transitions,[2] and the duration of the regime transitions is available in Table 1.

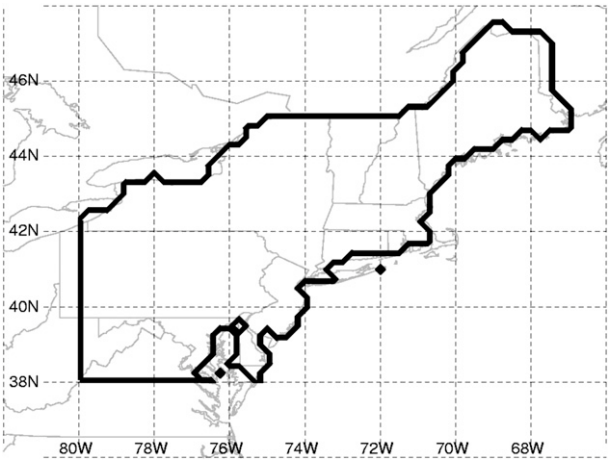

FIG. 1. The domain used to construct daily (1200–1200 UTC) domain-averaged NE precipitation time series from the NCEP Unified Precipitation Dataset.

Time series of 24-h (1200–1200 UTC) cool-season domain-averaged NE precipitation and standardized anomalies of domain-averaged NE precipitation are constructed for 1948–2003 from the 0.25° × 0.25° gridded NCEP Unified Precipitation Dataset (UPD; Higgins et al. 2000) over the region delineated in Fig. 1 following Archambault et al. (2008, see their section 2b). To construct the standardized NE precipitation anomaly time series, a power transformation is applied to the NE precipitation data to make the distribution approximately symmetric, and then daily anomalies are computed from the 1948–2003 climatology. The 24-h cool-season NE precipitation anomaly associated with each regime transition is computed by averaging the 24-h cool-season NE precipitation anomalies for all days falling within the regime transition, and it is tested for statistical significance using a two-sided Student's t test (e.g., Wilks 2006, see section 5.2.1). Based on results of the statistical analysis of NE precipitation to be shown next, 24-h periods associated with NE precipitation anomalies of at least +1.6 SD are defined as major NE precipitation events.[3]

b. Results

Table 2 displays the mean 24-h cool-season NE precipitation, anomaly, and anomaly statistical significance associated with each regime transition. Positive cool-season NE precipitation anomalies are associated with

[2] In each regime transition category, a small percentage of days (i.e., 2.6%–6.3%; not shown) also fall into another regime transition category.

[3] The 24-h NE precipitation anomaly threshold of +1.6 SD is relaxed relative to the +2.0 SD anomaly threshold used by Archambault et al. (2008) to define major NE precipitation events. This modification yields a larger sample size of events to be used in the composite analysis (section 3) than would be obtained using the +2.0 SD anomaly threshold.

TABLE 2. The mean 24-h cool-season NE precipitation, anomaly, and anomaly statistical significance associated with each regime transition.

Regime transition	Mean 24-h NE precipitation (mm)	Mean 24-h NE precipitation anomaly (SD)	Statistical significance (%)
NAO^+ to NAO^-	3.79	+0.23	99.9
NAO^- to NAO^+	2.32	−0.12	96.9
PNA^+ to PNA^-	1.84	−0.19	99.9
PNA^- to PNA^+	3.27	+0.20	99.9

NAO^+ to NAO^- and PNA^- to PNA^+ transitions, and negative cool-season NE precipitation anomalies are associated with NAO^- to NAO^+ and PNA^+ to PNA^- transitions. All four precipitation anomalies are statistically significant at the 95% level, with precipitation anomalies associated with NAO^+ to NAO^-, PNA^+ to PNA^-, and PNA^- to PNA^+ transitions significant at the 99.9% level. Stratifying the mean 24-h cool-season NE precipitation anomalies by month (Table 3) reveals that positive cool-season NE precipitation anomalies are associated with NAO^+ to NAO^- and PNA^- to PNA^+ transitions for five of the six cool-season months, whereas negative cool-season NE precipitation anomalies are associated with NAO^- to NAO^+ and PNA^+ to PNA^- transitions for four of the six months. Based upon the magnitude of the precipitation anomalies displayed in Table 3, NE precipitation is most favored to be above normal during NAO^+ to NAO^- transitions in November, December, and January and during PNA^- to PNA^+ transitions in November, March, and April. Conversely, NE precipitation is most favored to be below normal during NAO^- to NAO^+ transitions in November, December, and March and during PNA^+ to PNA^- transitions in December, January, and March.

To examine the distribution of cool-season NE precipitation during the four regime transitions, we construct 24-h cool-season NE precipitation anomaly distributions and distribution differences from cool-season climatology (Fig. 2). Figures 2a,b reveal that NAO^+ to NAO^- transitions are associated with a markedly increased frequency of major NE precipitation events (i.e., 24-h periods with precipitation anomalies exceeding +1.6 SD). The frequency of major cool-season NE precipitation events during each type of regime transition and for climatology is shown in Table 4. During NAO^+ to NAO^- transitions, 13.3% of 24-h periods are categorized as major NE precipitation events, nearly twice the climatological frequency of 6.8%. Figures 2g,h indicate that PNA^- to PNA^+ transitions are associated with a noticeably increased frequency of moderate NE precipitation events (i.e., 24-h periods associated with +0.8 to +1.6 SD precipitation anomalies). In contrast to the other two regime transitions, NAO^- to NAO^+ transitions (Figs. 2c,d) and PNA^+ to PNA^- transitions (Figs. 2e,f) are associated with an overall decreased frequency of NE precipitation events associated with a positive precipitation anomaly. Compared to climatology, the frequency of major NE precipitation events (Table 4) is close to normal during NAO^- to NAO^+ and PNA^- to PNA^+ transitions (6.7% and 7.4%, respectively) and well below normal during PNA^+ to PNA^- transitions (3.6%).

3. Composite analysis

a. Methodology and data

A composite analysis of major NE precipitation events occurring during NAO^+ to NAO^- transitions is conducted so that the statistical association established in section 2b between NAO^+ to NAO^- transitions and a markedly increased frequency of major cool-season NE precipitation events can be explored in a synoptic–dynamic framework. The procedure to select events for compositing begins with consideration of the 30 major NE precipitation events that occur during NAO^+ to NAO^- transitions (Table 4). If consecutive 24-h periods meet the definition of a major NE precipitation event, only the first 24-h period is considered for compositing, yielding 24 nonconsecutive major NE precipitation events in 42 NAO^+ to NAO^- transitions. Next, NAO index criteria are imposed to objectively identify major NE precipitation events associated with similar large-scale flow evolutions. Since, as shown in Table 5, the NAO phase is considerably more likely to be positive

TABLE 3. The mean 24-h cool-season NE precipitation anomaly associated with each regime transition by month.

	NE precipitation anomaly (SD)			
	NAO^+ to NAO^-	NAO^- to NAO^+	PNA^+ to PNA^-	PNA^- to PNA^+
Nov	+0.32	−0.15	−0.04	+0.42
Dec	+0.36	−0.28	−0.34	+0.03
Jan	+0.43	+0.33	−0.47	+0.18
Feb	+0.09	+0.03	+0.12	−0.01
Mar	−0.08	−0.39	−0.27	+0.28
Apr	+0.25	−0.03	+0.02	+0.33

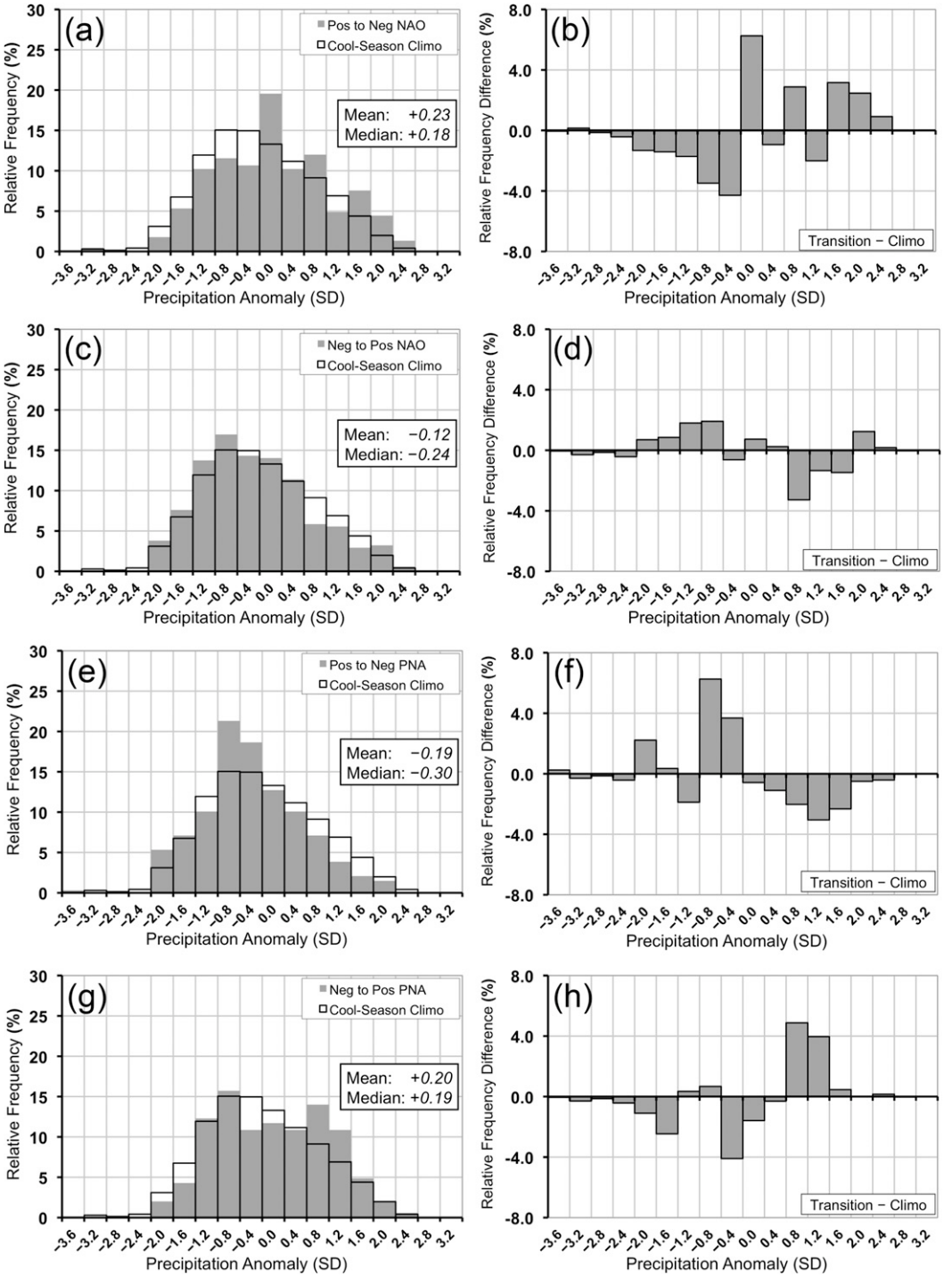

FIG. 2. The relative frequency (%) of 24-h cool-season NE precipitation anomalies during (a) NAO^+ to NAO^-, (c) NAO^- to NAO^+, (e) PNA^+ to PNA^-, and (g) PNA^- to PNA^+ transitions (shaded); and the relative frequency difference from cool-season climatology (%) during (b) NAO^+ to NAO^-, (d) NAO^- to NAO^+, (f) PNA^+ to PNA^-, and (h) PNA^- to PNA^+ transitions. The cool-season climatological relative frequency (%) of 24-h NE precipitation anomalies (not shaded) is included in (a),(c),(e), and (g) for comparison with the relative frequency of cool-season NE precipitation anomalies during regime transitions.

TABLE 4. The fraction of 24-h cool-season periods classified as major cool-season NE precipitation events, and the frequency and frequency difference from climatology of major cool-season NE precipitation events, for climatology and each regime transition.

	Major cool-season NE precipitation events		
	Fraction of 24-h periods	Frequency (%)	Frequency diff from climatology (%)
Climatology	690/10 150	6.8	—
NAO^+ to NAO^-	30/225	13.3	+6.5
NAO^- to NAO^+	22/331	6.7	−0.1
PNA^+ to PNA^-	12/338	3.6	−3.2
PNA^- to PNA^+	26/350	7.4	+0.6

TABLE 5. The daily NAO index distribution at the onset (T+0 h) of the 24 nonconsecutive major cool-season NE precipitation events occurring during NAO^+ to NAO^- transitions.

Daily NAO index at T+0 h	No. of precipitation events
−1.5 to −1.0	2
−1.0 to −0.5	2
−0.5 to 0.0	3
0.0 to +0.5	5
+0.5 to +1.0	4
+1.0 to +1.5	8

than negative at the onset of nonconsecutive major cool-season NE precipitation events (i.e., T+0 h) occurring during NAO^+ to NAO^- transitions, the 17 major NE precipitation events with a positive NAO index at T+0 h are considered for compositing. Of these 17 events, 14 are retained after requiring that the NAO index be negative by T+48 h. Finally, of these 14 major NE precipitation events, 11 are selected for compositing after subjectively determining that the 500-hPa flow evolution associated with these events is similar. The predominant synoptic features of the composite, to be documented in section 3b, also are present in composites constructed from subsets of the 11 events grouped arbitrarily (i.e., in chronological order; not shown), implying that the 11-event composite is sufficiently insensitive to the inclusion or exclusion of particular events. Table 6 shows the onset dates and the NE precipitation amounts and anomalies for the 11 major cool-season NE precipitation events chosen for compositing, as well as the periods of the associated NAO^+ to NAO^- transitions.

Sets of composite analyses are constructed at 24-h intervals from the 2.5° NCEP–NCAR reanalysis for the 5-day period (T−48 h to T+72 h) surrounding the onset of the major NE precipitation event (T+0 h). The four sets of analyses display 500-hPa geopotential height and departures from climatology (Fig. 3a); potential temperature θ and wind speed on the dynamic tropopause (DT; 2.0-PVU surface; Fig. 3b); 1000–500-hPa thickness, 700-hPa absolute vorticity, and SLP (Fig. 4a); and column-integrated precipitable water (PW), 700-hPa vertical motion ω, and 700-hPa wind (Fig. 4b). The 500-hPa geopotential height departures are calculated from a 1948–2003 15-day running mean climatology constructed from the NCEP–NCAR reanalysis, with statistical significance assessed using a two-sided Student's t test following Archambault et al. (2008, see their section 2c).

b. Results

Figures 3 and 4 reveal that a dramatic evolution from a zonal flow pattern to a high-latitude blocking pattern takes place over eastern North America and the North Atlantic surrounding the composite NAO^+ to NAO^- NE precipitation event. At T−48 h, a high-latitude North Atlantic trough and a midlatitude eastern U.S./western North Atlantic ridge are evident in the 500-hPa geopotential height (Fig. 3a) and DT θ (Fig. 3b) fields. The flow pattern at T−48 h promotes strong midlatitude westerlies on the DT (Fig. 3b) and at 700 hPa (Fig. 4b) that extend from approximately 90° to 30°W. Over North America, a ridge–trough–ridge pattern comprising a western U.S. ridge, a central North America trough, and the aforementioned eastern U.S./western North Atlantic ridge (Figs. 3a,b) is indicative of a Rossby wave train.

The wave train pattern over North America amplifies substantially in tandem with surface cyclogenesis in the 48 h prior to the onset of the NE precipitation event, while the flow pattern over the North Atlantic remains relatively zonal. As the western U.S. ridge weakens slightly, the trough–ridge couplet over central and eastern North America strengthens and progresses eastward to the eastern United States and western North Atlantic between T−48 h and T+0 h (Figs. 3a,b). Just downstream of the central North American trough axis, a surface low is apparent over the Great Lakes at T−24 h (Fig. 4a). The surface low deepens while moving eastward over the next 24 h, and warm-air advection suggested by the SLP and 1000–500-hPa thickness fields develops over the NE and eastern Canada by T+0 h (Fig. 4a). At T−24 h and T+0 h, the surface low coincides with an implied local maximum in quasigeostrophic (QG) forcing for ascent due to advection of 700-hPa cyclonic absolute vorticity by the 1000–500-hPa thermal wind (e.g., Trenberth 1978; Fig. 4a). At T−24 h, the surface low is near the poleward entrance region of a jet streak on the DT, and at T+0 h is collocated with both the equatorward entrance region of this jet streak and the poleward exit region of a second jet streak on the DT rounding the

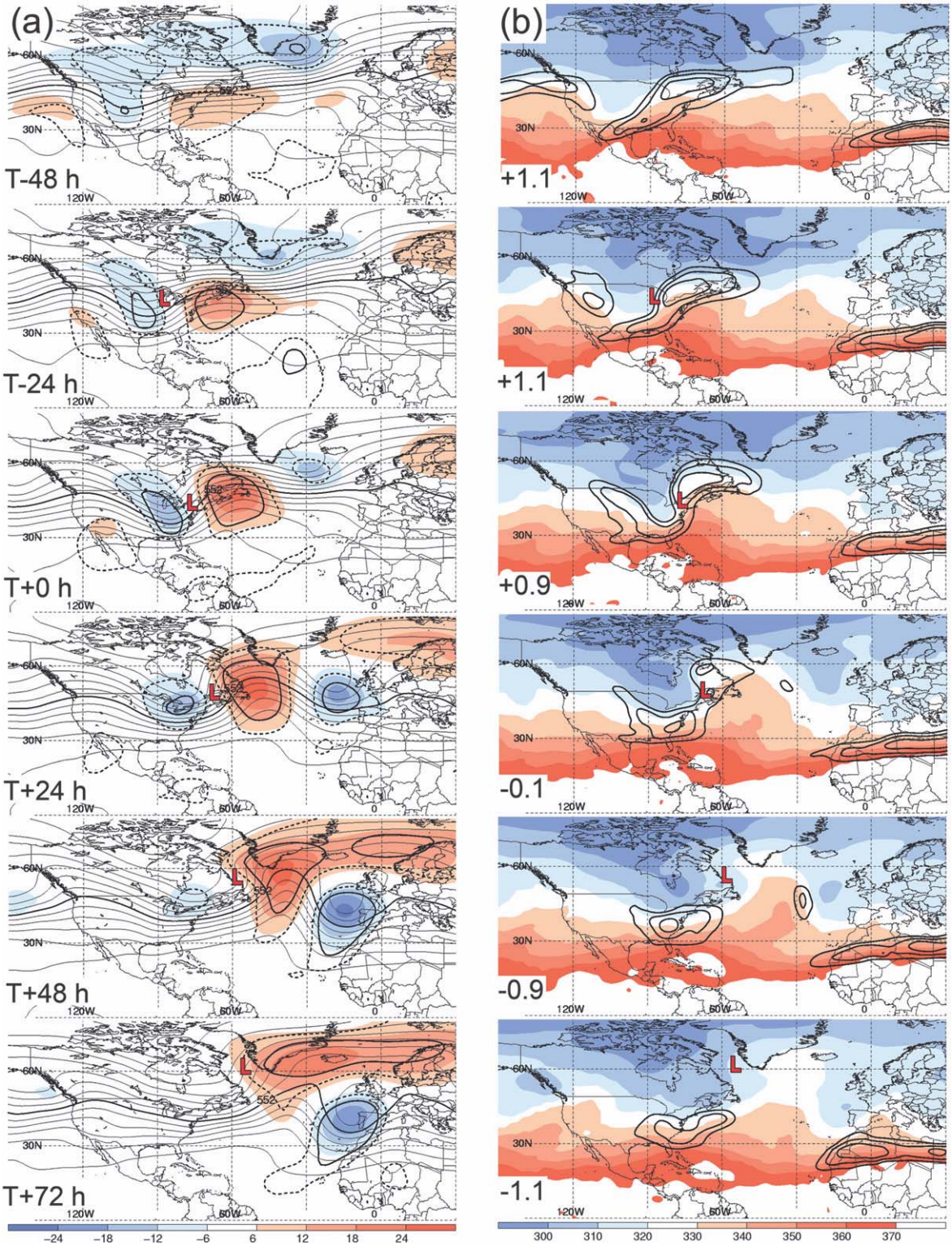

FIG. 3. Composite analyses of the 5-day period surrounding the onset of a major cool-season NE precipitation event (T+0 h) associated with a NAO^+ to NAO^- transition. Analyses show (a) 500-hPa geopotential height (solid; every 6 dam, with the 552-dam contour shown as a thick line) and departures from climatology (shaded; every 6 dam according to the color bar), with thick dashed (solid) contours denoting statistical significance at the 95% (99%) confidence level; and (b) DT θ (shaded; every 10 K according to the color bar) and wind speed (solid; every 5 m s^{-1} beginning at 35 m s^{-1}). The analysis time relative to the onset of the precipitation event is indicated in the bottom-left corner of each analysis in (a), and the composite daily NAO index (SD) is indicated in the bottom-left corner of each analysis in (b). The "L" symbol denotes the position of the key surface low in (a) and (b).

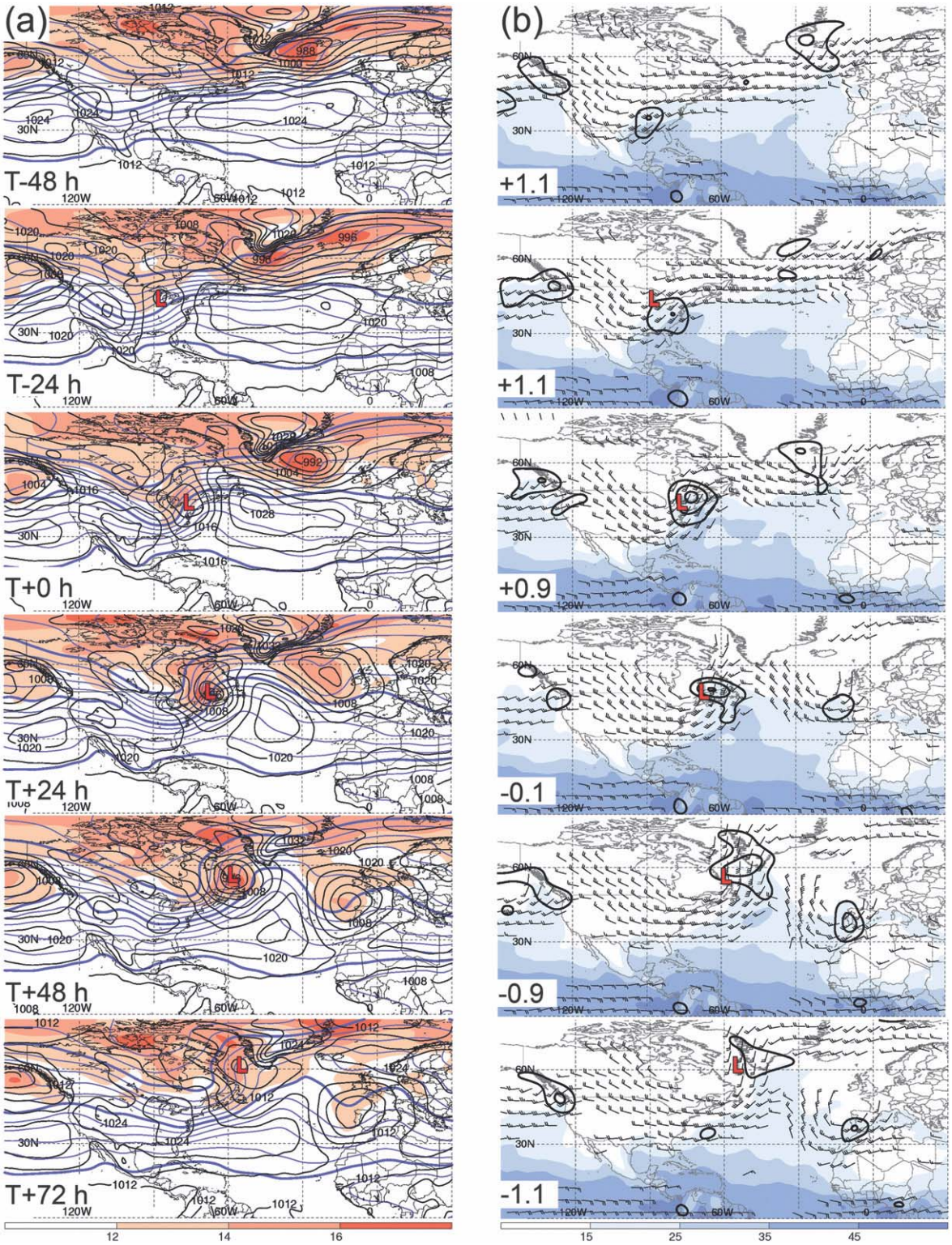

FIG. 4. As in Fig. 3, but for (a) 1000–500-hPa thickness (solid blue; every 6 dam, with the 510-, 540-, and 570-dam contours shown as thick lines), 700-hPa absolute vorticity (shaded; beginning at 12×10^{-5} s^{-1} according to the color bar), and SLP (solid black; every 4 hPa); and (b) PW (shaded; beginning at 15 mm according to the color bar), 700-hPa ω (solid; every 1×10^{-3} hPa s^{-1}, negative values only), and 700-hPa wind (barbs; plotted where speeds exceed 7.5 m s^{-1}).

base of the upstream trough (Fig. 3b). The collocation of the surface low with equatorward jet entrance and poleward jet exit regions is a common signature of cool-season precipitation events in the eastern United States (e.g., Uccellini and Kocin 1987; Archambault et al. 2008).

Consistent with the implied QG forcing for ascent, an area of 700-hPa ascent encompasses the southeastern U.S. and Mid-Atlantic region at T−24 h, and reaches the NE and southeastern Canada by T+0 h (Fig. 4b). A plume of high PW extending from the Gulf of Mexico up the eastern U.S. coast accompanies the 700-hPa ascent at T−24 h and T+0 h (Fig. 4b). At T+0 h, the 1000–500-hPa thickness over most of the NE exceeds 540 dam, suggesting that rain is the predominant precipitation type.

In the 72-h period following the onset of the NE precipitation event, a high-latitude blocking pattern develops over the North Atlantic. Between T+0 h and T+48 h, the trough upstream of the NE surface low acquires a negative tilt (Figs. 3a,b), and at T+48 h cyclonic wave breaking is indicated by a sign reversal of the meridional DT θ gradient at about 55°N over eastern Canada and the northwestern North Atlantic (Fig. 3b). The ridge downstream of the NE surface low strengthens and expands poleward between T+0 h and T+48 h (Figs. 3a,b) as lower-tropospheric warm-air advection overspreads the Canadian Maritimes and northwestern North Atlantic (Fig. 4a). As the surface low moves poleward in conjunction with the negatively tilted trough between T+0 h and T+48 h, it decouples from the jet entrance and exit regions: the upstream jet streak is nearly stationary over the eastern United States and western North Atlantic, and the downstream jet streak rapidly dissipates (Fig. 3b). The surface low, however, continues to coincide with an implied local maximum in the advection of 700-hPa cyclonic absolute vorticity by the 1000–500-hPa thermal wind (Fig. 4a). The region of 700-hPa ascent and the PW plume accompanying the low persist between T+0 h and T+48 h on the western flank of the downstream ridge over the western North Atlantic (Fig. 4b).

The development of blocked flow over the North Atlantic also apparently arises from the retrogression and intensification of a separate ridge over the northeastern North Atlantic. This evolution occurs as above-normal 500-hPa geopotential heights over Scandinavia at T+0 h expand westward in the following 72 h and merge with the area of above-normal 500-hPa geopotential heights in the crest of the western North Atlantic ridge by T+48 h (Fig. 3a). Southwest of the retrograding ridge, a trough over the eastern North Atlantic narrows and deepens, ultimately spawning a cutoff cyclone that approaches the northwestern coast of the Iberian Peninsula by T+48 h (Figs. 3a,b).

By T+72 h, a high-latitude blocking pattern has become established over the North Atlantic, as indicated by above-normal 500-hPa geopotential heights across the high-latitude North Atlantic and below-normal 500-hPa geopotential heights over the eastern midlatitude North Atlantic (Fig. 3a). The surface low that impacted the NE has reached 60°N over the Davis Strait and continues to be accompanied by an area of ascent (Fig. 4b). A split-flow pattern has developed over the eastern North Atlantic, with belts of enhanced 500-hPa geopotential height (Fig. 3a) and DT θ (Fig. 3b) gradients along the crest of the high-latitude ridge and along the base of the midlatitude cutoff cyclone.

4. Case study

a. Methodology and data

A case study of a major cool-season NE precipitation event associated with a NAO^+ to NAO^- transition is performed to allow synoptic signatures suggested by the composite analysis of such events to be examined in greater detail. The 29–30 November 1963 NE rainstorm (Table 6) is chosen for study because the synoptic pattern evolution surrounding this major NE precipitation event closely resembles the composite evolution. This event set all-time daily precipitation records for 29 November at 12 first-order observing stations in the NE, ranging from 75.4 mm at Watertown, New York, to 34.0 mm at Newark, New Jersey (National Climatic Data Center; see online at http://www7.ncdc.noaa.gov/IPS/lcd/lcd.html). Of the 11 major NE precipitation events in the composite, this event ranks second in storm-total NE precipitation (not shown). This event also is of interest from the standpoint that Danielsen (1966) demonstrated the utility of isentropic backward trajectories in an analysis of the dry slot of the cyclone associated with this precipitation event. To facilitate comparison with the composite, the same 5-day sequences of analyses (T−48 h to T+72 h; 1200 UTC 27 November–1200 UTC 2 December 1963) are produced for the case study as for the composite. To better resolve synoptic features, the case study is performed using the 1.125° 40-yr European Centre for Medium-Range Weather Forecasts (ECMWF) Re-Analysis (ERA-40) reanalysis (Uppala et al. 2005) rather than the 2.5° NCEP–NCAR reanalysis used in the composite analysis, with the exception that the climatology used to calculate 500-hPa geopotential height departures is constructed from the NCEP–NCAR reanalysis as in section 3a.

A distinctive synoptic signature of the 29–30 November 1963 NE rainstorm, to be identified in section 4b, is the amplification of a high-latitude North Atlantic ridge that occurs in conjunction with a NAO^+ to NAO^-

TABLE 6. The 11 major cool-season NE precipitation events occurring during NAO^+ to NAO^- transitions chosen for compositing. The case study is boldface.

Major NE precipitation event onset date (T+0 h; 1200 UTC)	NE precipitation for 24-h period following onset date (mm)	NE precipitation anomaly for 24-h period following onset date (SD)	Period of transition
27 Dec 1949	9.2	+1.7	25–30 Dec
3 Nov 1951	27.1	+2.3	3–5 Nov
29 Nov 1963	**14.2**	**+1.8**	**29 Nov–2 Dec**
15 Dec 1968	12.2	+1.8	14–17 Dec
14 Mar 1980	14.8	+2.0	14–17 Mar
1 Apr 1987	13.2	+1.7	1–3 Apr
3 Dec 1991	20.9	+2.3	28 Nov–4 Dec
19 Jan 1996	15.6	+2.4	19–21 Jan
9 Nov 1996	30.4	+2.4	6–12 Nov
11 Jan 2000	12.5	+2.0	10–14 Jan
17 Dec 2000	20.2	+2.4	16–21 Dec

transition. A diabatic contribution to this high-latitude ridge amplification will be diagnosed in terms of PV nonconservation by plotting regions of 300-hPa negative parcel PV tendency for the 60-h period following the onset of the major NE precipitation event (T+0 h to T+60 h; 1200 UTC 29 November–0000 UTC 2 December 1963). The 300-hPa parcel PV tendency is evaluated using 1.125° ERA-40 reanalysis data by summing the 300-hPa local, horizontal advective, and vertical advective contributions:

$$\frac{d\mathrm{PV}}{dt} = \frac{\partial \mathrm{PV}}{\partial t_p} + \mathbf{V} \cdot \nabla_p \mathrm{PV} + \omega \frac{\partial \mathrm{PV}}{\partial p}. \qquad (1)$$

The local contribution to the parcel PV tendency at a given time, T_0, is evaluated by subtracting the PV field at $T_{-6\mathrm{h}}$ from the PV field at $T_{+6\mathrm{h}}$ and dividing by 12 h. The horizontal advective contribution to the parcel PV tendency is smoothed using a 1–2–1 temporal filter [i.e., $(T_{-6\mathrm{h}} + 2T_0 + T_{+6\mathrm{h}})/4$]. To illustrate the transport of low-PV air into the amplifying high-latitude ridge over the North Atlantic and to provide additional evidence of a diabatic contribution to ridge amplification, nine kinematic backward trajectories ending in the 300-hPa ridge crest at 1200 UTC 1 December 1963 (T+48 h) are calculated. The trajectory calculation uses a 1-h time step, with the three-dimensional velocity components linearly interpolated spatially and temporally to the parcel position from 6-h 1.125° ERA-40 reanalysis data.

b. Results

Figures 5–8 illustrate the synoptic evolution for the 5-day period encompassing the 29–30 November 1963 NE rainstorm case study and the NAO^+ to NAO^- transition associated with this major cool-season NE precipitation event. At T−48 h, zonal flow at 500 hPa prevails over the North Atlantic, consistent with a NAO^+ pattern, as well as across the eastern North Pacific and North America (Fig. 5a). At this time, a weak surface low just north of the western Great Lakes (Fig. 7a) is embedded in west-northwesterly flow at 500 and 700 hPa (Figs. 5a and 8a). By T−24 h, the surface low has deepened slightly in the presence of advection of 700-hPa cyclonic absolute vorticity by the 1000–500-hPa thermal wind (Fig. 7a) associated with an amplifying upper-tropospheric trough over south-central Canada (Figs. 5a and 6a). Upstream of this trough, a ridge has developed along the western North American coast. Meanwhile, a second surface low has formed near the central Gulf Coast (Fig. 7a) just downstream of a cutoff cyclone over the south-central United States (Fig. 5a) near the tip of a zonally oriented DT θ streamer (Fig. 6a). Compared to the northern surface low, the southern surface low coincides with weaker cyclonic vorticity advection by the thermal wind and higher PW values (Figs. 7a and 8a).

Between T−24 h and T+0 h, the south-central Canadian trough merges with the south-central U.S. cutoff cyclone to form a deep trough over the east-central United States (Figs. 5a and 6a). Upstream of the east-central U.S. trough, the ridge that developed along the western North American coast at T−24 h amplifies, while a ridge develops over eastern North America and the western North Atlantic. The development of the eastern North American/western North Atlantic ridge occurs in conjunction with warm-air advection in advance of the northern and southern surface lows (Fig. 7a). The formation of this ridge–trough–ridge pattern is indicative of downstream development accompanying the leading edge of a Rossby wave train approaching from the North Pacific. At T+0 h, coinciding with the onset of the major NE precipitation event, the southern surface low is located at the tip of a cyclonically curved DT θ tongue over the southeastern United States, and is in close proximity to the poleward exit region of a jet

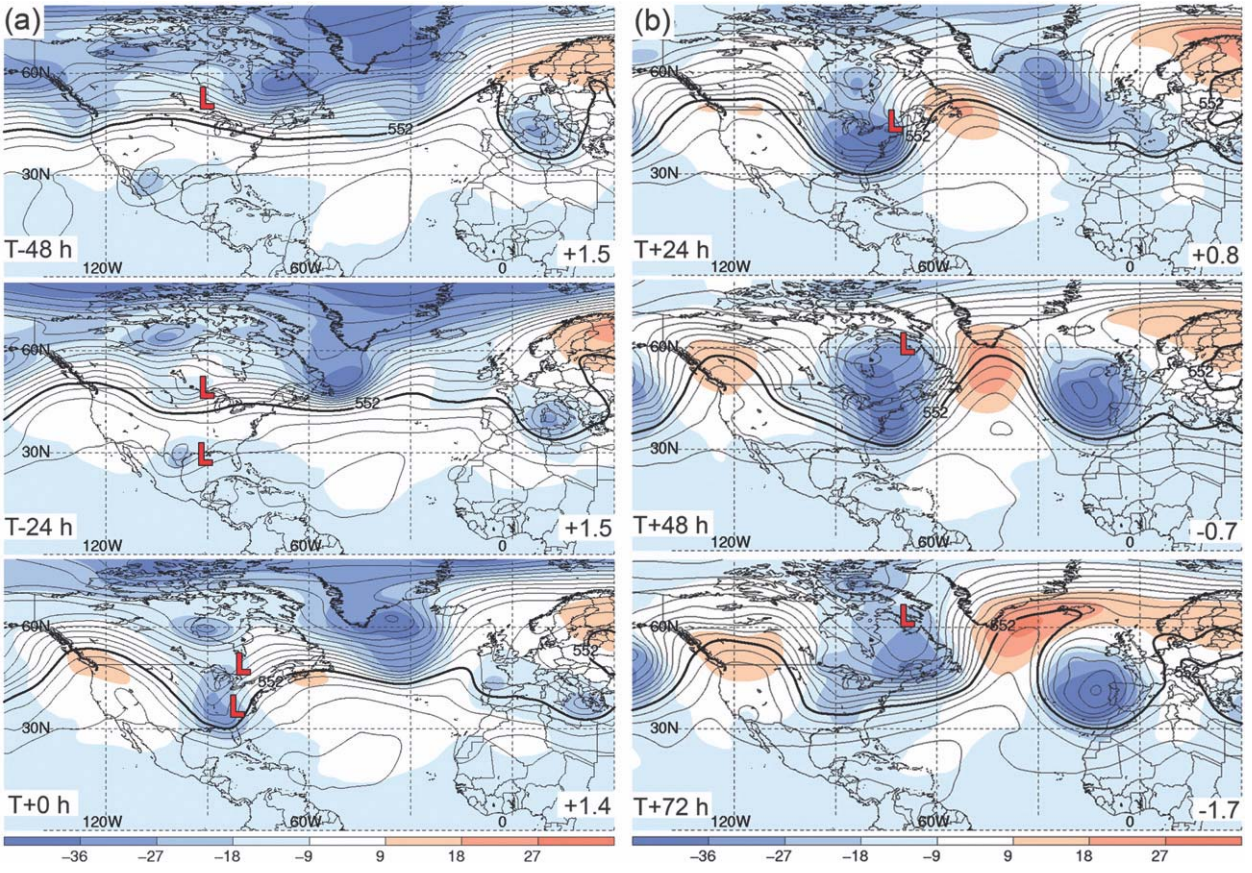

FIG. 5. Analyses of 500-hPa geopotential height (solid; every 6 dam, with the 552-dam contour shown as a thick line) and departures from climatology (shaded; every 9 dam according to the color bar) for the 5-day period surrounding the onset of a major cool-season NE precipitation event associated with a NAO^+ to NAO^- transition: (a) T−48 h to T+0 h (1200 UTC 27 Nov–1200 UTC 29 Nov 1963) and (b) T+24 h to T+72 h (1200 UTC 30 Nov–1200 UTC 2 Dec 1963). The analysis time relative to the onset of the precipitation event and the daily NAO index (SD) are indicated in the bottom-left and bottom-right corners of each analysis, respectively. The "L" symbol denotes the position of the key surface lows in each analysis.

streak over the south-central United States (Fig. 6a). The northern surface low is positioned just downstream of a DT θ minimum over the western Great Lakes and is collocated with the equatorward entrance region of a jet streak over eastern Canada. Advection of 700-hPa cyclonic absolute vorticity by the 1000–500-hPa thermal wind, 700-hPa ascent, and high PW values associated with the southern surface low encompass the southeastern U.S. and Mid-Atlantic region (Figs. 7a and 8a). Cyclonic vorticity advection by the thermal wind accompanying the northern surface low is comparable (Fig. 7a), but 700-hPa ascent is less vigorous and PW values are relatively lower than their counterparts in the southern surface low (Fig. 8a).

Between T+0 h and T+24 h, the northern and southern surface lows merge, resulting in an intense surface low over the NE (Fig. 7b) accompanied by a negatively tilted trough–ridge couplet (Fig. 5b) and marked cyclonic wave breaking over eastern North America at T+24 h (Fig. 6b). This surface-low merger is reminiscent of the January 1978 Ohio Valley wave-merger cyclogenesis event (Hakim et al. 1995, 1996) and the March 1993 "Superstorm" (Bosart et al. 1996). At T+24 h, the NE surface low is positioned beneath both the poleward-exit and equatorward-entrance regions of cyclonically and anticyclonically curved jet streaks, respectively (Fig. 6b), and is collocated with pronounced advection of 700-hPa cyclonic absolute vorticity by the 1000–500-hPa thermal wind (Fig. 7b). The presence of vigorous ascent and the poleward transport of high PW by strong 700-hPa winds over the NE (Fig. 8b) is consistent with the copious rainfall amounts associated with this major precipitation event.

Between T+24 h and T+48 h, ridge amplification occurs over eastern Canada and the high-latitude North Atlantic (Figs. 5b and 6b) coincident with a broad area of strong warm-air advection over the Canadian Maritimes and the Labrador Strait accompanying the surface low,

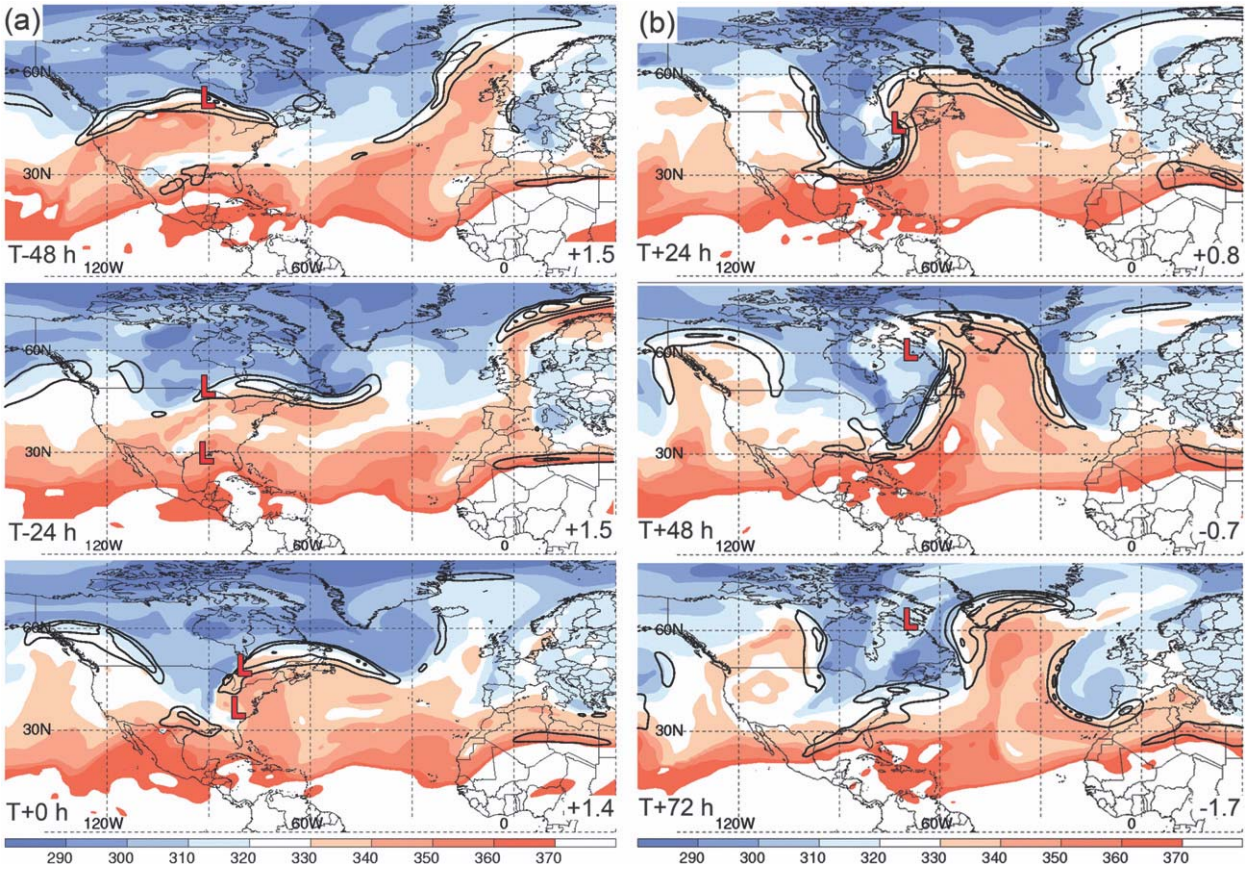

FIG. 6. As in Fig. 5, but for DT θ (shaded; every 10 K according to the color bar) and wind speed (solid; every 10 m s^{-1} beginning at 50 m s^{-1}).

which deepens rapidly during this period (Fig. 7b). The presence of a poleward-directed PW plume and 700-hPa ascent (Fig. 8b) over the high-latitude North Atlantic suggests that diabatic heating may be contributing to the ridge amplification. Distinct cyclonic wave breaking occurs over eastern North America and the western North Atlantic in conjunction with the rapidly deepening surface low between T+24 h and T+48 h, with the DT θ field exhibiting a ''treble clef'' signature characteristic of occluded cyclones (Martin 1998) (Fig. 6b). During this time period, the upper-tropospheric flow over the North Atlantic becomes increasingly blocked, consistent with an NAO index decrease from +0.8 to −0.7 between T+24 h and T+48 h (Figs. 5b and 6b). Contributing to the blocked flow is a 500-hPa cutoff cyclone over the midlatitude eastern North Atlantic at T+48 h (Fig. 5b), which develops as a DT θ streamer extends southeastward downstream of the amplifying high-latitude North Atlantic ridge between T+0 h and T+24 h and then wraps up cyclonically near the northwest Iberian Peninsula coast by T+48 h (Figs. 6a,b).

By T+72 h, a NAO$^-$ pattern characterized by blocked flow over the North Atlantic has become established (Fig. 5b). The blocked flow consists of above-normal 500-hPa geopotential heights in the crest and downstream of the high-latitude North Atlantic ridge, and below-normal 500-hPa geopotential heights in association with the midlatitude eastern North Atlantic cutoff cyclone. The surface low that previously impacted the NE has decoupled from the DT jet entrance and exit regions and weakened between T+48 h and T+72 h (Figs. 6b and 7b). During this period, a long fetch of 700-hPa southerly winds has maintained the PW plume along the western flank of the high-latitude North Atlantic ridge, and 700-hPa ascent persists at the tip of the PW plume over southern Greenland (Fig. 8b).

The synoptic evolution surrounding the 29–30 November 1963 NE rainstorm case study closely resembles the synoptic evolution surrounding the composite NAO$^+$ to NAO$^-$ NE precipitation event in the following respects: At T−48 h, relatively zonal flow prevails over the North Atlantic, consistent with a NAO$^+$ pattern, as well as over North America (Figs. 3a and 5a). Between

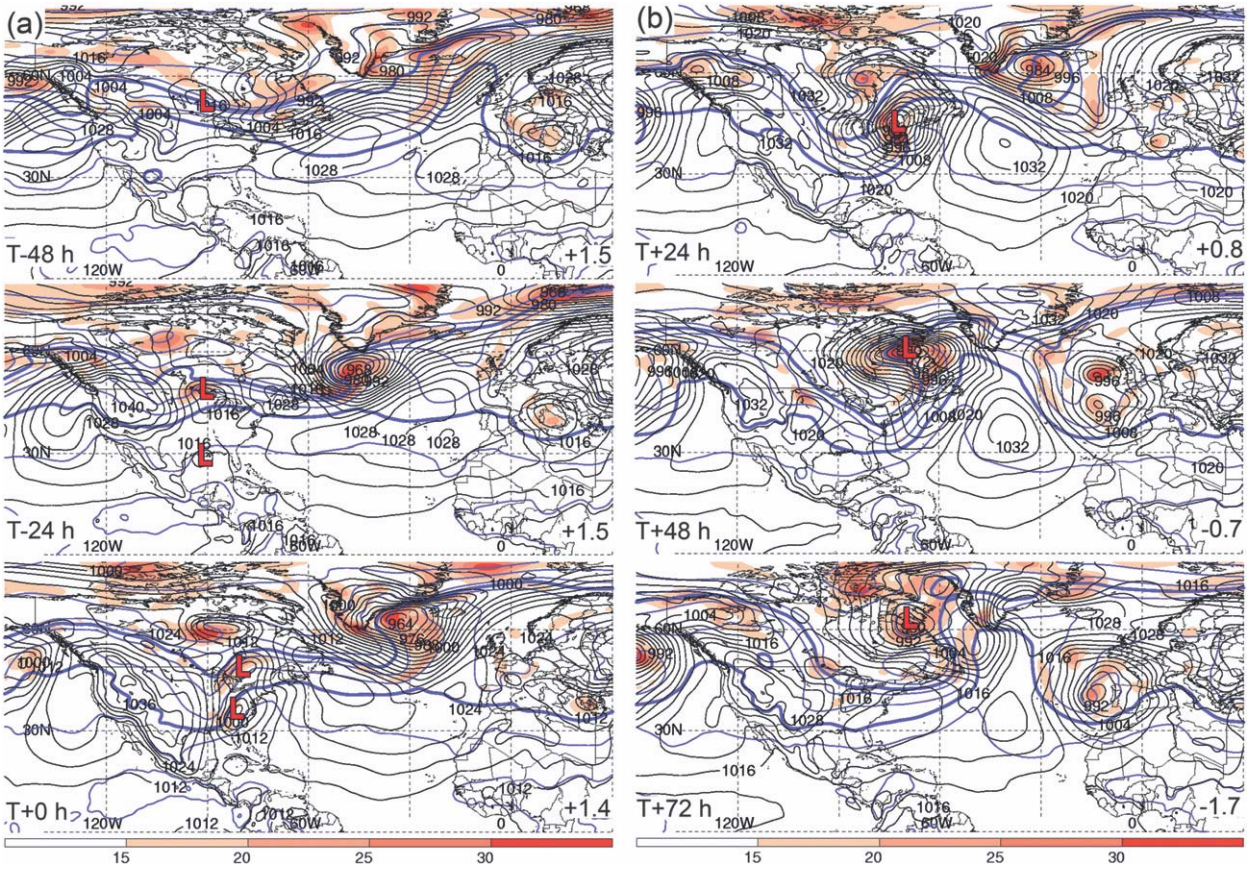

FIG. 7. As in Fig. 5, but for 1000–500-hPa thickness (solid blue; every 6 dam, with the 510- and 540-dam contours shown as thick lines), 700-hPa absolute vorticity (shaded; beginning at 15×10^{-5} s^{-1} according to the color bar), and SLP (solid black; every 8 hPa).

T−48 h and T+0 h, a Rossby wave train migrating from the North Pacific is associated with the formation of a trough over central and eastern North America (Figs. 3a,b and Figs. 5a,6a). Downstream of the central-eastern North American trough, a surface low develops beneath the equatorward-entrance region of a jet streak in the presence of cyclonic vorticity advection by the thermal wind (Figs. 3b,4a and Figs. 6a,7a). By T+24 h, a region of ascent and the tip of a plume of high PW accompany the surface low (Figs. 4b and 8b), which is departing the NE and is located beneath equatorward-entrance and poleward-exit regions of distinct jet streaks (Figs. 3b and 6b). Between T+24 h and T+48 h, the surface low moves poleward over eastern Canada in advance of the central-eastern North American trough, and warm-air advection accompanying the surface low contributes to the development and amplification of a high-latitude North Atlantic ridge (Figs. 3a,4a and Figs. 5b,7b). Also during this time period, the region of ascent and PW plume accompanying the surface low move poleward along the western flank of the amplifying high-latitude North Atlantic ridge (Figs. 4b and 8b). Between T+24 h and T+48 h, the central-eastern North American trough and the high-latitude North Atlantic ridge acquire a negative tilt indicative of cyclonic wave breaking (Figs. 3b and 6b), and a midlatitude cutoff cyclone forms over the eastern North Atlantic downstream of the ridge (Figs. 3a and 5b). By T+72 h, a NAO$^-$ pattern characterized by blocked North Atlantic flow has become established (Figs. 3a and 5b).

In addition to exhibiting various synoptic signatures suggested by the composite analysis, the case study reveals key details of the synoptic pattern evolution that are not resolved by the compositing procedure. In the case study, the surface low associated with the major NE precipitation event deepens explosively between T+0 h and T+24 h over the eastern United States and Canada following the merger of separate surface lows (Figs. 7a,b), whereas in the composite analysis no merger is apparent and the surface low that impacts the NE deepens slightly between T+0 h and T+24 h (Fig. 4a). Moreover, cyclonic wave breaking over eastern North America and the western North Atlantic at T+24 h and T+48 h is more pronounced in the case study (Fig. 6b) than in the

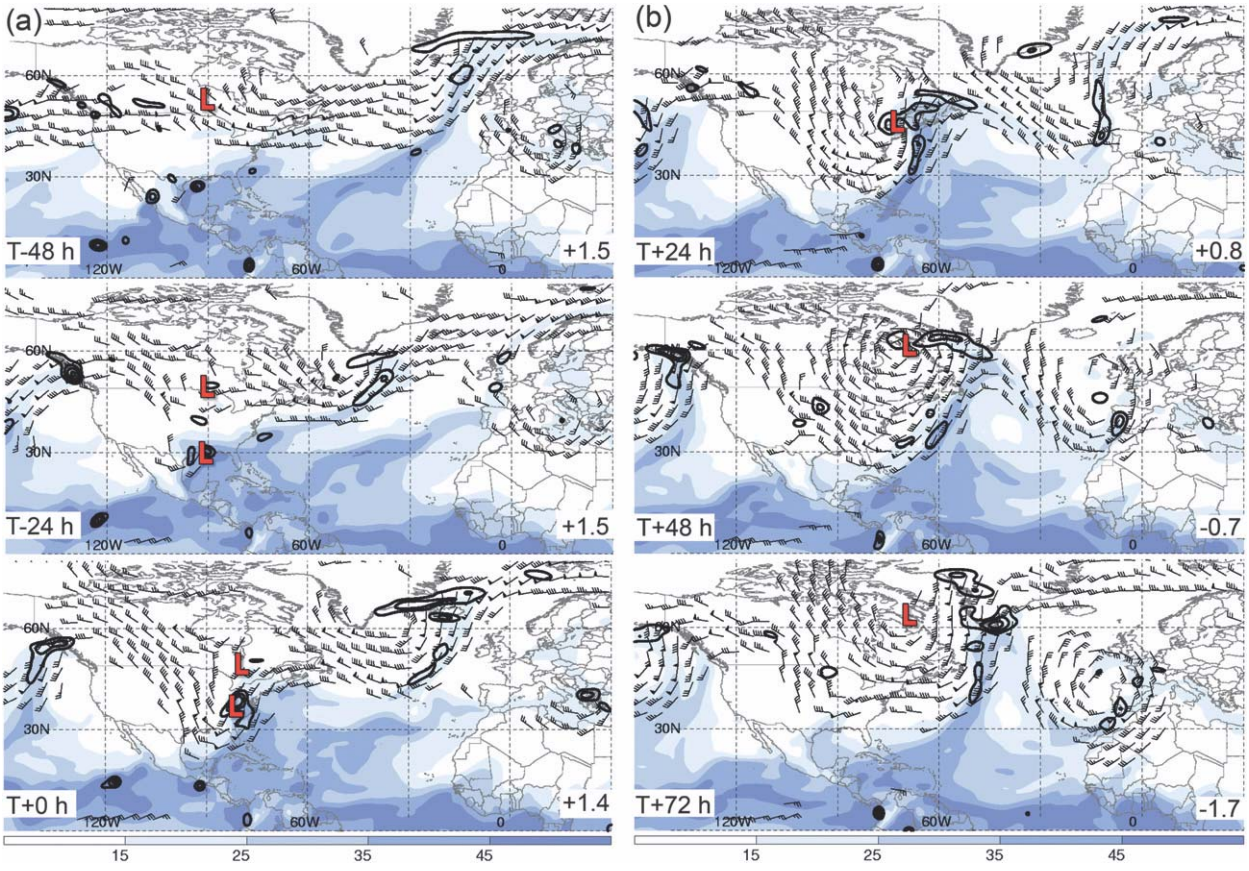

FIG. 8. As in Fig. 5, but for PW (shaded; beginning at 15 mm according to the color bar), 700-hPa ω (solid; every 5×10^{-3} hPa s^{-1}, negative values only), and 700-hPa wind (barbs; plotted where speeds exceed 12.5 m s^{-1}).

composite (Fig. 3b), and the PW plume on the western flank of the amplifying North Atlantic ridge between T+0 h and T+72 h is more clearly defined in the case study (Figs. 8a,b) than in the composite (Fig. 4b).

The diabatic contribution to high-latitude ridge amplification over the North Atlantic accompanied by cyclonic wave breaking suggested in the case study is now diagnosed in terms of PV nonconservation for the 60-h period following the onset of the major NE precipitation event. A diabatic contribution to high-latitude ridge amplification is evident in the collocation of negative 300-hPa parcel PV tendencies with regions of ascent and high PW on the upstream flank and in the crest of the ridge between T+0 h and T+60 h (Fig. 9). During this time period, negative PV advections are found primarily on the downstream flank of the ridge, with maximum values generally about twice the maximum values of the negative parcel PV tendencies [i.e., -10.0 PVU $(12\ \text{h})^{-1}$ versus -5.0 PVU $(12\ \text{h})^{-1}$]. Between T+0 h and T+24 h, negative 300-hPa parcel PV tendencies are collocated with ascent over the eastern United States, as well as with ascent to the north over eastern Canada (Fig. 9a). At T+36 h and T+48 h, negative parcel PV tendencies are collocated with the crest of the amplifying North Atlantic ridge and a broad region of ascent associated with the surface low that previously impacted the NE (Figs. 7b and 9b). At T+60 h, the area of negative parcel PV tendencies is located over southern Greenland and continues to be collocated with ascent (Fig. 9b). The presence of negative 300-hPa parcel PV tendencies in the ridge crest between T+36 h and T+48 h suggests that diabatic heating may be impeding the eastward translation of the ridge crest and contributing to the negative tilting of the ridge accompanying cyclonic wave breaking by opposing the effect of negative PV advection. During this period, the tip of the ridge crest is nearly stationary at approximately 78°W in a region of negative parcel PV tendencies, while the forward flank of the ridge surges northeastward across southern Greenland in the presence of negative PV advection (Fig. 9b).

A backward trajectory analysis is conducted to diagnose the transport of low-PV air into the amplifying ridge over the high-latitude North Atlantic (Fig. 10a) and to provide additional evidence of a diabatic contribution

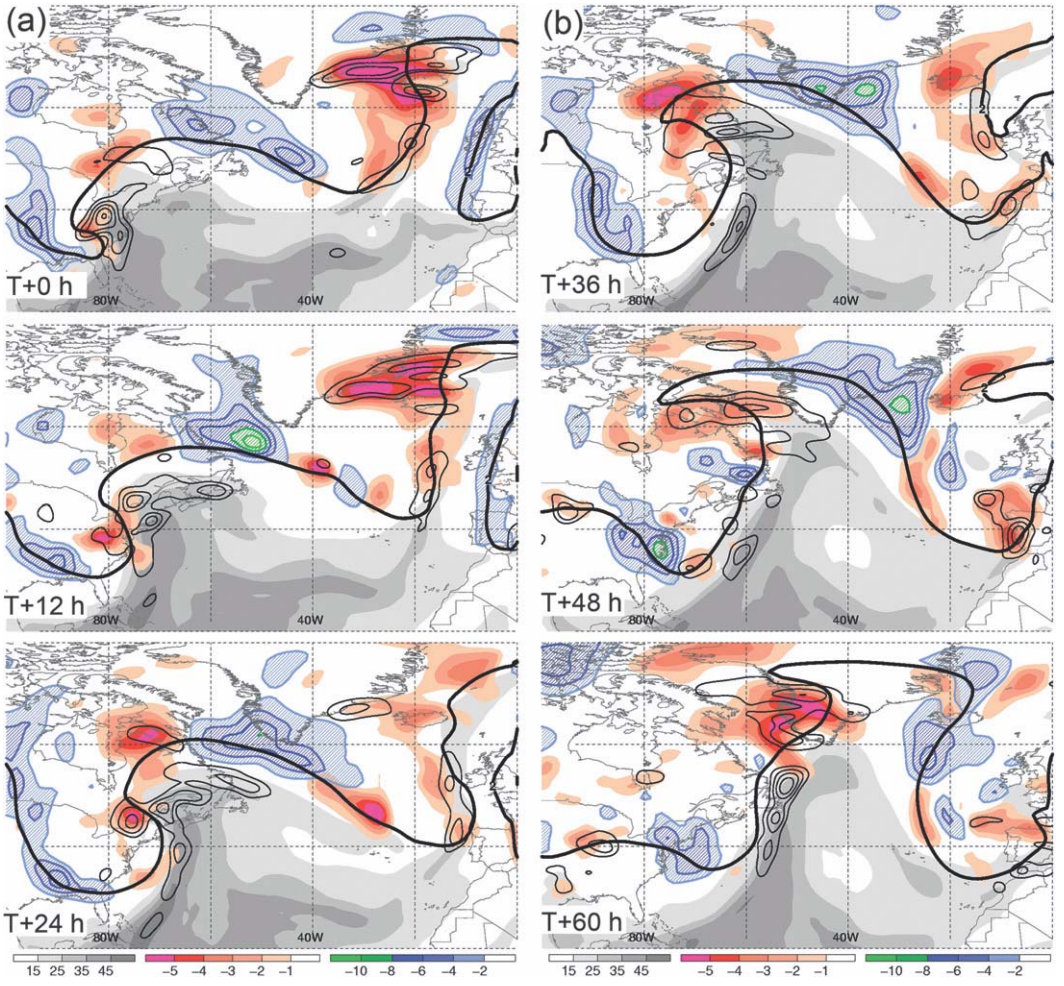

FIG. 9. Analyses of PW (shaded; beginning at 15 mm according to the left color bar), 700–500-hPa layer-averaged ω (solid; every 3×10^{-3} hPa s^{-1} starting at -3×10^{-3} hPa s^{-1}, negative values only), 300-hPa parcel PV tendency [shaded; beginning at -1.0 PVU (12 h)$^{-1}$ according to the center color bar], 300-hPa PV advection [hatched; beginning at -2.0 PVU (12 h)$^{-1}$ according to the right color bar], and 300-hPa 2.0-PVU contour (solid) for the 2.5-day period following the onset of a major cool-season NE precipitation event associated with a NAO^+ to NAO^- transition: (a) T+0 h to T+24 h (1200 UTC 29 Nov–1200 UTC 30 Nov 1963) and (b) T+36 h to T+60 h (0000 UTC 1 Dec–0000 UTC 2 Dec 1963). The analysis time relative to the onset of the precipitation event is indicated in the bottom-left corner of each analysis.

to ridge amplification (Fig. 10b). Figure 10a indicates that parcels ending in the 300-hPa ridge crest over the high-latitude North Atlantic at T+48 h originate over the Gulf of Mexico and the south-central United States at T+0 h. Between T+0 h and T+48 h, the parcels move northeastward and then turn anticyclonically as low-PV air surges poleward in conjunction with ridge development, amplification, and cyclonic wave breaking, as indicated by the evolution of the 2.0-PVU contour at 300 hPa (Fig. 10a). This poleward surge of low-PV air at 300 hPa corresponds to a surge of DT θ values in excess of 320 K over eastern North America and the western North Atlantic between T+0 h and T+48 h (Figs. 6a,b). Figure 10b shows that seven of nine air parcels originate between 390 and 510 hPa, with two parcels originating at 650 and 750 hPa. Between T+0 h and T+42 h, the θ values of the seven parcels originating between 390 and 510 hPa are nearly constant, whereas the θ values of the two parcels that originate at 650 and 750 hPa increase from 313 and 305 K to 322 K. The increase in θ, and increase then decrease in PV, of the latter two parcels between T+36 h and T+42 h is suggestive of air ascending through a midtropospheric diabatic heating maximum associated with condensation. Between T+42 h and T+48 h, all nine parcels ascend 70–100 hPa, increase their θ values by 2–3 K, and decrease their PV values by

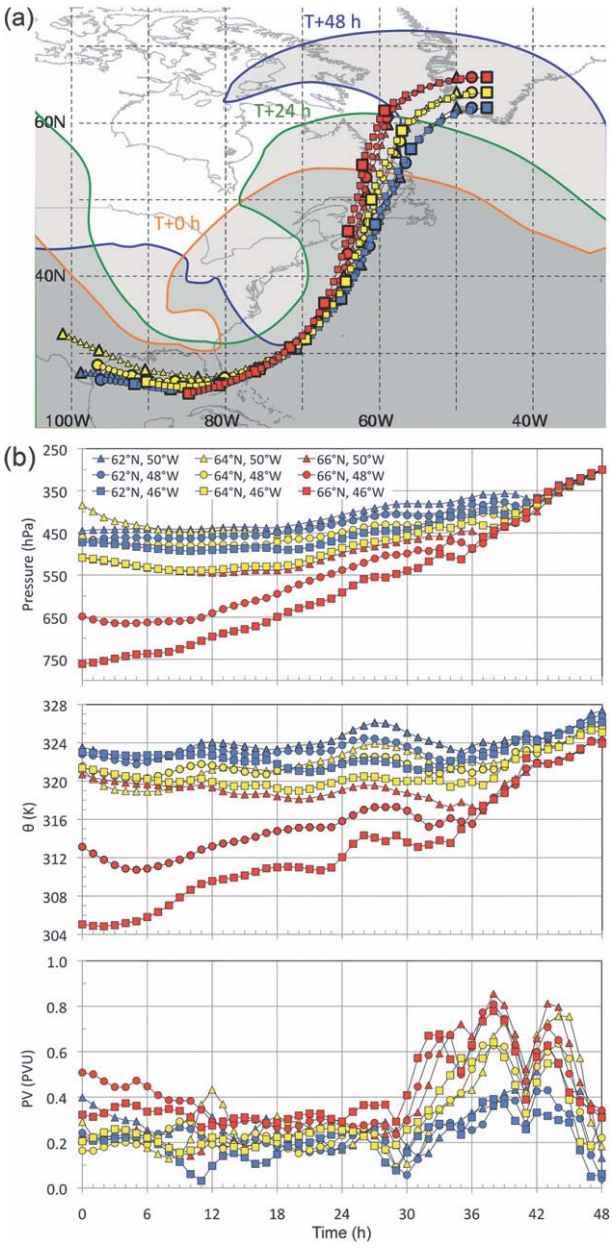

FIG. 10. Nine 48-h kinematic backward trajectories ending in a 4.0° × 4.0° box centered at 64°N, 48°W at T+48 h (1200 UTC 1 Dec 1963): (a) The 2.0-PVU contour at 300 hPa for T+0 h (1200 UTC 29 Nov), T+24 h (1200 UTC 30 Nov), and T+48 h (1200 UTC 1 Dec; regions where PV is less than 2.0 PVU are shaded), overlaid with 1-h time step parcel trajectories (larger markers denote 0000, 0600, 1200, and 1800 UTC positions), and (b) corresponding time series of parcel pressure (hPa), θ (K), and PV (PVU) between T+0 h and T+48 h.

0.4–0.6 PVU (Fig. 10b). The θ increase and PV decrease of the parcels as they ascend between T+42 h and T+48 h suggests a diabatic contribution to upper-tropospheric ridge amplification over the North Atlantic.

5. Discussion

An analysis of daily cool-season NE precipitation during objectively identified NAO and PNA regime transitions shows that statistically significant relationships exist between each regime transition type and cool-season NE precipitation. Based on this analysis, NAO^+ to NAO^- and PNA^- to PNA^+ transitions favor relatively wet conditions in the NE, whereas NAO^- to NAO^+ and PNA^+ to PNA^- transitions favor relatively dry conditions. During NAO^+ to NAO^- transitions, major NE precipitation events occur nearly twice as frequently as usual, and tend to commence when the NAO phase is positive (i.e., at the beginning of the transitions). While none of the other regime transitions is associated with more frequent major NE precipitation events, PNA^- to PNA^+ transitions are associated with more frequent moderate NE precipitation events. It is speculated that this association may be explained by an increased frequency of NE cold-frontal passages during PNA^- to PNA^+ transitions. This speculation is supported by studies showing that successive cold-frontal passages tend to occur during eastern U.S. cold-air outbreaks, which are characterized by the development of a deep eastern North American trough resembling a PNA^+ pattern (e.g., Konrad and Colucci 1989). A general implication of the statistical findings is that precipitation is more (less) frequent in the NE when the surrounding large-scale flow pattern is evolving from zonal to amplified (amplified to zonal) on a synoptic time scale.

The relationship between major NE precipitation events and NAO^+ to NAO^- transitions is explored from a synoptic–dynamic perspective by performing a composite analysis and case study of the 5-day period surrounding a major cool-season NE precipitation event associated with a NAO^+ to NAO^- transition. Results reveal that a surface cyclone accompanying the major NE precipitation event helps to produce a high-latitude North Atlantic ridge, which corresponds to the onset of a North Atlantic blocking pattern and a strong NAO^- phase. The correspondence between the onset of a North Atlantic blocking pattern and the onset of a strong NAO^- phase supports the interpretation of the NAO by Woollings et al. (2008) as an alternation between a ''basic state'' (i.e., a NAO^+ phase) and ''blocked state'' (i.e., a NAO^- phase).

The implication that an individual cyclone can initiate a North Atlantic blocking pattern is supported by previous studies linking upstream cyclones to the onset of blocking (e.g., Colucci 1985, 1987; Pelly and Hoskins 2003a). In the composite and case study, the cyclone associated with a major NE precipitation event during a

NAO^+ to NAO^- transition helps to build a high-latitude North Atlantic ridge by producing prolonged warm-air advection at high latitudes and facilitating the poleward transport of high DT-θ air (or, alternatively, upper-tropospheric low-PV air) in conjunction with cyclonic wave breaking. In addition to these adiabatic processes, the case study indicates that diabatic heating accompanying a PW plume may help to build the high-latitude ridge. In the case study, PV nonconservation collocated with ascent and high PW is identified along the western flank and in the crest of the ridge as it amplifies. A trajectory analysis shows that a source region of upper-tropospheric low-PV air in the ridge crest is the lower-tropospheric subtropics, and that this air experiences an increase in θ, and an increase then decrease in PV, as it streams poleward and ascends. This behavior is characteristic of air rising through a midtropospheric diabatic heating maximum associated with condensation (e.g., Wernli and Davies 1997; Massacand et al. 2001) and suggests a diabatic contribution to upper-tropospheric low PV in the ridge. The findings of this study thus are consistent with previous work that collectively highlights the importance of both adiabatic (e.g., Crum and Stevens 1988; Nakamura and Wallace 1993) and diabatic (e.g., Massacand et al. 2001; Lazear 2007; Croci-Maspoli and Davies 2009) processes in the onset of blocking.

As previously noted, cyclonic wave breaking over eastern North America and the western North Atlantic is a characteristic of NAO^+ to NAO^- transitions associated with major NE precipitation events. This finding is consistent with recent studies showing that eastern North American/western North Atlantic cyclonic wave breaking is the critical mechanism for the generation of a NAO^- pattern (e.g., Benedict et al. 2004; Franzke et al. 2004; Martius et al. 2007; Rivière and Orlanski 2007; Altenhoff et al. 2008; Luo et al. 2008; Woollings et al. 2008). Specifically, Rivière and Orlanski (2007) showed that negative meridional eddy momentum fluxes associated with a cyclonic wave breaking event accompanying a major snowstorm over the eastern United States could promote the onset of a NAO^- pattern by weakening the North Atlantic jet stream and displacing it equatorward. Furthermore, the finding of the composite analysis and case study that a Rossby wave train migrating from the North Pacific across North America is a common feature of NAO^+ to NAO^- transitions associated with major NE precipitation events is in agreement with studies identifying downstream development across the Pacific–North American sector as a precursor to cyclonic wave breaking and North Atlantic blocking (e.g., Altenhoff et al. 2008; Woollings et al. 2008).

An additional characteristic of NAO^+ to NAO^- transitions associated with major NE precipitation events identified in this study is the formation of a cutoff cyclone associated with a DT-θ streamer (i.e., PV streamer; Appenzeller and Davies 1992) over the midlatitude eastern North Atlantic. The presence of ascent and enhanced PW over the Iberian Peninsula accompanying the cutoff cyclone in the composite analysis and case study at T+48 h (Figs. 4b and 8b) implies that Iberian Peninsula precipitation events may be favored during NAO^+ to NAO^- transitions. These results are consistent with studies showing that precipitation events associated with cutoff cyclones are favored downstream of blocks (e.g., Robertson and Ghil 1999; Carrera et al. 2004), as well as with studies linking PV streamers, which also occur preferentially downstream of blocks (e.g., Altenhoff et al. 2008), to heavy precipitation events (e.g., Massacand et al. 2001; Martius et al. 2006).

6. Summary and conclusions

This observational study investigates relationships between large-scale regime transitions, which are defined using daily NAO and PNA indices, and major cool-season (November–April) NE precipitation events. A 1948–2003 statistical analysis of daily cool-season NE precipitation during NAO and PNA transitions reveals that above-normal precipitation is associated with NAO^+ to NAO^- and PNA^- to PNA^+ transitions and below-normal precipitation is associated with NAO^- to NAO^+ and PNA^+ to PNA^- transitions. Major NE precipitation events are found to occur at nearly twice the climatological frequency during NAO^+ to NAO^- transitions, and at about half the climatological frequency during PNA^+ to PNA^- transitions. When considered with the study of Archambault et al. (2008), which found no clear statistical relationships between NAO and PNA regimes and the frequency of major NE precipitation events, or between NAO regimes and cool-season NE precipitation anomalies, the present study suggests that NAO and PNA regime transitions may be more strongly related to cool-season NE precipitation than are NAO and PNA regimes.

The finding that major cool-season NE precipitation events are substantially more frequent during NAO^+ to NAO^- transitions is explored via a composite analysis and a case study. The composite analysis of 11 major cool-season NE precipitation events occurring during NAO^+ to NAO^- transitions indicates that a cyclone and cyclonic wave breaking accompanying the major NE precipitation event play a critical role in establishing a high-latitude North Atlantic ridge associated with the onset of a NAO^- pattern by facilitating strong warm-air advection and a poleward surge of high θ on the DT. A case study of the 5-day period encompassing the 29–30

November 1963 NE rainstorm, one of the major NE precipitation events in the composite, indicates that in addition to adiabatic processes, diabatic processes are important in establishing the North Atlantic ridge. Diagnosis of PV nonconservation and a trajectory analysis suggest that diabatic heating may contribute to the development of upper-tropospheric low PV within the North Atlantic ridge. The finding that a cyclone accompanied by a major NE precipitation event can play a critical role in a NAO^+ to NAO^- transition serves to illustrate that large-scale flow reconfigurations such as the onset of high-latitude blocking, which can significantly influence regional climates on intraseasonal time scales, sometimes can be related to the occurrence of a single weather event.

Given that global forecast models often exhibit skill in predicting large-scale regime transitions at lead times of a week or more, it is anticipated that the statistical relationships between NAO and PNA regime transitions and cool-season NE precipitation documented in this study will be useful in the medium-range forecasting of the likelihood of NE precipitation. As a point of caution in the operational application of the relationship between major cool-season NE precipitation events and NAO^+ to NAO^- transitions, it should be recognized that NAO^+ to NAO^- transitions often occur without major NE precipitation events, and, conversely, that major NE precipitation events often occur without NAO^+ to NAO^- transitions. A noteworthy example of the latter is the March 1993 ''Superstorm'' (e.g., Bosart et al. 1996; Rivière and Orlanski 2007), which occurred in conjunction with a NAO^- to NAO^+ transition. In this case, a pronounced downstream ridge developed over the midlatitude North Atlantic in conjunction with anticyclonic wave breaking, resulting in an intensified North Atlantic jet stream (i.e., a NAO^+ phase) rather than blocked North Atlantic flow (i.e., a NAO^- phase). An additional point of caution is that since the onset of blocking may correspond to a reduction in model forecast skill (e.g., Tibaldi et al. 1997; Pelly and Hoskins 2003b), NAO^+ to NAO^- transitions may be relatively challenging to predict. An avenue of future work is to investigate model forecast skill associated with NAO^+ to NAO^- transitions relative to that of other regime transitions.

Acknowledgments. The authors thank Dr. Anantha Aiyyer at North Carolina State University for providing the programs used to compute trajectories and create the precipitation and teleconnection index time series employed in this study, and Ross Lazear at the University at Albany, SUNY, for his helpful suggestions during the preparation of this manuscript. In addition, thanks are due to Kevin Tyle and Dr. David Knight at the University at Albany, SUNY, for providing technical support, and to three anonymous reviewers, whose insightful comments and suggestions helped improve the clarity of this manuscript. This work is derived from a portion of the first author's M.S. thesis at the University at Albany, SUNY, and was supported by NOAA Grant NA07WA0458 and National Science Foundation Grant ATM-0434189.

REFERENCES

Altenhoff, A. M., O. Martius, M. Croci-Maspoli, C. Schwierz, and H. C. Davies, 2008: Linkage of atmospheric blocks and synoptic-scale Rossby waves: A climatological analysis. *Tellus,* **60A,** 1053–1063.

Appenzeller, C., and H. C. Davies, 1992: Structure of stratospheric intrusions into the troposphere. *Nature,* **358,** 570–572.

Archambault, H. M., L. F. Bosart, D. Keyser, and A. R. Aiyyer, 2008: Influence of large-scale flow regimes on cool-season precipitation in the northeastern United States. *Mon. Wea. Rev.,* **136,** 2945–2963.

Barnston, A. G., and R. E. Livezey, 1987: Classification, seasonality and persistence of low-frequency atmospheric circulation patterns. *Mon. Wea. Rev.,* **115,** 1083–1126.

Benedict, J. J., S. Lee, and S. B. Feldstein, 2004: Synoptic view of the North Atlantic Oscillation. *J. Atmos. Sci.,* **61,** 121–144.

Berrisford, P., B. J. Hoskins, and E. Tyrlis, 2007: Blocking and Rossby wave breaking on the dynamical tropopause in the Southern Hemisphere. *J. Atmos. Sci.,* **64,** 2881–2898.

Black, R. X., and R. M. Dole, 1993: The dynamics of large-scale cyclogenesis over the North Pacific Ocean. *J. Atmos. Sci.,* **50,** 421–442.

Bosart, L. F., G. J. Hakim, K. R. Tyle, M. A. Bedrick, W. E. Bracken, M. J. Dickinson, and D. M. Schultz, 1996: Large-scale antecedent conditions associated with the 12–14 March 1993 cyclone (''Superstorm '93'') over eastern North America. *Mon. Wea. Rev.,* **124,** 1865–1891.

Carrera, M. L., R. W. Higgins, and V. E. Kousky, 2004: Downstream weather impacts associated with atmospheric blocking over the northeast Pacific. *J. Climate,* **17,** 4823–4839.

Coleman, J. S., and J. C. Rogers, 2003: Ohio River valley winter moisture conditions associated with the Pacific–North American teleconnection pattern. *J. Climate,* **16,** 969–981.

Colucci, S. J., 1985: Explosive cyclogenesis and large-scale circulation changes: Implications for atmospheric blocking. *J. Atmos. Sci.,* **42,** 2701–2717.

——, 1987: Comparative diagnosis of blocking versus nonblocking planetary-scale circulation changes during synoptic-scale cyclogenesis. *J. Atmos. Sci.,* **44,** 124–139.

Croci-Maspoli, M., and H. C. Davies, 2009: Key dynamical features of the 2005/06 European winter. *Mon. Wea. Rev.,* **137,** 664–678.

——, C. Schwierz, and H. C. Davies, 2007: Atmospheric blocking: Space–time links to the NAO and PNA. *Climate Dyn.,* **29,** 713–725.

Crum, F. X., and D. E. Stevens, 1988: A case study of atmospheric blocking using isentropic analysis. *Mon. Wea. Rev.,* **116,** 223–241.

Dai, A., I. Y. Fung, and A. D. Del Genio, 1997: Surface observed global land precipitation variations during 1900–88. *J. Climate,* **10,** 2943–2962.

Danielsen, E. F., 1966: Research in four-dimensional diagnosis of cyclonic storm cloud systems. Scientific Rep. 1, Air Force Cambridge Research Laboratories AFCRL 66-30, 52 pp. [NTIS AD-632668.]

Dole, R. M., 1986a: Persistent anomalies of the extratropical Northern Hemisphere wintertime circulation: Structure. *Mon. Wea. Rev.,* **114,** 178–207.

——, 1986b: The life cycles of persistent anomalies and blocking over the North Pacific. *Advances in Geophysics,* Vol. 29, Academic Press, 31–69.

——, 2008: Linking weather and climate. *Synoptic–Dynamic Meteorology and Weather Analysis and Forecasting: A Tribute to Fred Sanders, Meteor. Monogr.,* No. 55, Amer. Meteor. Soc., 297–348.

——, and N. D. Gordon, 1983: Persistent anomalies of the extratropical Northern Hemisphere wintertime circulations: Geographic distribution and regional persistence characteristics. *Mon. Wea. Rev.,* **111,** 1567–1586.

——, and R. X. Black, 1990: Life cycles of persistent anomalies. Part II: The development of persistent negative height anomalies over the North Pacific Ocean. *Mon. Wea. Rev.,* **118,** 824–826.

Feldstein, S. B., 2002: Fundamental mechanisms of the growth and decay of the PNA teleconnection pattern. *Quart. J. Roy. Meteor. Soc.,* **128,** 775–796.

——, 2003: The dynamics of NAO teleconnection pattern growth and decay. *Quart. J. Roy. Meteor. Soc.,* **129,** 901–924.

Franzke, C., S. Lee, and S. B. Feldstein, 2004: Is the North Atlantic Oscillation a breaking wave? *J. Atmos. Sci.,* **61,** 145–160.

Hakim, G. J., L. F. Bosart, and D. Keyser, 1995: The Ohio Valley wave-merger cyclogenesis event of 25–26 January 1978. Part I: Multiscale case study. *Mon. Wea. Rev.,* **123,** 2663–2692.

——, D. Keyser, and L. F. Bosart, 1996: The Ohio Valley wave-merger cyclogenesis event of 25–26 January 1978. Part II: Diagnosis using quasigeostrophic potential vorticity inversion. *Mon. Wea. Rev.,* **124,** 2176–2205.

Higgins, R. W., and S. D. Schubert, 1994: Simulated life cycles of persistent anticyclonic anomalies over the North Pacific: Role of synoptic-scale eddies. *J. Atmos. Sci.,* **51,** 3238–3259.

——, W. Shi, E. Yarosh, and R. Joyce, 2000: *Improved United States Precipitation Quality Control System and Analysis*. NCEP/Climate Prediction Center Atlas 7, 45 pp. [Available online at http://www.cpc.ncep.noaa.gov/research_papers/ncep_cpc_atlas/7/index.html.]

Hurrell, J. W., 1995: Decadal trends in the North Atlantic Oscillation: Regional temperatures and precipitation. *Science,* **269,** 676–679.

Johansson, Å., 2007: Prediction skill of the NAO and PNA from daily to seasonal time scales. *J. Climate,* **20,** 1957–1975.

Kalnay, E., and Coauthors, 1996: The NCEP/NCAR 40-Year Reanalysis Project. *Bull. Amer. Meteor. Soc.,* **77,** 437–471.

Kistler, R., and Coauthors, 2001: The NCEP–NCAR 50-Year Reanalysis: Monthly means CD-ROM and documentation. *Bull. Amer. Meteor. Soc.,* **82,** 247–267.

Konrad, C. E., and S. J. Colucci, 1989: An examination of extreme cold air outbreaks over eastern North America. *Mon. Wea. Rev.,* **117,** 2687–2700.

Lau, N.-C., 1988: Variability of the observed midlatitude storm tracks in relation to low-frequency changes in the circulation pattern. *J. Atmos. Sci.,* **45,** 2718–2743.

Lazear, R. A., 2007: The effects of diabatic heating on upper-tropospheric anticyclogenesis. M.S. thesis, Department of Atmospheric and Oceanic Sciences, University of Wisconsin—Madison, 78 pp.

Leathers, D. J., B. Yarnal, and M. A. Palecki, 1991: The Pacific/North American teleconnection pattern and United States climate. Part I: Regional temperature and precipitation associations. *J. Climate,* **4,** 517–527.

Löptien, U., and E. Ruprecht, 2005: Effect of synoptic systems on the variability of the North Atlantic Oscillation. *Mon. Wea. Rev.,* **133,** 2894–2904.

Luo, D., A. R. Lupo, and H. Wan, 2007a: Dynamics of eddy-driven low-frequency dipole modes. Part I: A simple model of North Atlantic Oscillations. *J. Atmos. Sci.,* **64,** 3–28.

——, T. Gong, and A. R. Lupo, 2007b: Dynamics of eddy-driven low-frequency dipole modes. Part II: Free mode characteristics of NAO and diagnostic study. *J. Atmos. Sci.,* **64,** 29–51.

——, ——, and Y. Diao, 2008: Dynamics of eddy-driven low-frequency dipole modes. Part IV: Planetary and synoptic wave-breaking processes during the NAO life cycle. *J. Atmos. Sci.,* **65,** 737–765.

Martin, J. E., 1998: The structure and evolution of a continental winter cyclone. Part I: Frontal structure and the occlusion process. *Mon. Wea. Rev.,* **126,** 303–328.

Martius, O., C. Schwierz, and H. C. Davies, 2006: Episodes of alpine heavy precipitation with an overlying elongated stratospheric intrusion: A climatology. *Int. J. Climatol.,* **26,** 1149–1164.

——, ——, and ——, 2007: Breaking waves at the tropopause in the wintertime Northern Hemisphere: Climatological analyses of the orientation and the theoretical LC1/2 classification. *J. Atmos. Sci.,* **64,** 2576–2592.

Massacand, A. C., H. Wernli, and H. C. Davies, 2001: Influence of upstream diabatic heating upon an Alpine event of heavy precipitation. *Mon. Wea. Rev.,* **129,** 2822–2828.

Mullen, S. L., 1986: The local balances of vorticity and heat for blocking anticyclones in a spectral general circulation model. *J. Atmos. Sci.,* **43,** 1406–1441.

Nakamura, H., and J. M. Wallace, 1993: Synoptic behavior of baroclinic eddies during the blocking onset. *Mon. Wea. Rev.,* **121,** 1892–1903.

Notaro, M., W.-C. Wang, and W. Gong, 2006: Model and observational analysis of the northeast U.S. regional climate and its relationship to the PNA and NAO patterns during early winter. *Mon. Wea. Rev.,* **134,** 3479–3505.

Orlanski, I., 2005: A new look at the Pacific storm track variability: Sensitivity to tropical SSTs and to upstream seeding. *J. Atmos. Sci.,* **62,** 1367–1390.

Pelly, J. L., and B. J. Hoskins, 2003a: A new perspective on blocking. *J. Atmos. Sci.,* **60,** 743–755.

——, and ——, 2003b: How well does the ECMWF Ensemble Prediction System predict blocking? *Quart. J. Roy. Meteor. Soc.,* **129,** 1683–1702.

Rex, D. F., 1950a: Blocking action in the middle troposphere and its effects upon regional climate I. An aerological study of blocking action. *Tellus,* **2,** 196–211.

——, 1950b: Blocking action in the middle troposphere and its effects upon regional climate II. The climatology of blocking action. *Tellus,* **2,** 275–301.

Rivière, G., and I. Orlanski, 2007: Characteristics of the Atlantic storm-track eddy activity and its relation with the North Atlantic Oscillation. *J. Atmos. Sci.,* **64,** 241–266.

Robertson, A. W., and M. Ghil, 1999: Large-scale weather regimes and local climate over the western United States. *J. Climate,* **12,** 1796–1813.

Rogers, J. C., 1990: Patterns of low-frequency monthly sea level pressure variability (1899–1986) and associated wave cyclone frequencies. *J. Climate,* **3,** 1364–1379.

Sanders, F., and J. R. Gyakum, 1980: The synoptic-dynamic climatology of the ''bomb.'' *Mon. Wea. Rev.,* **108,** 1589–1606.

Shabbar, A., J. Huang, and K. Higuchi, 2001: The relationship between the wintertime North Atlantic Oscillation and blocking episodes in the North Atlantic. *Int. J. Climatol.,* **21,** 355–369.

Shutts, G. J., 1983: The propagation of eddies in diffluent jetstreams: Eddy vorticity forcing of 'blocking' flow fields. *Quart. J. Roy. Meteor. Soc.,* **109,** 737–761.

——, 1986: A case study of eddy forcing during an Atlantic blocking episode. *Advances in Geophysics,* Vol. 29, Academic Press, 135–161.

Sisson, P. A., and J. R. Gyakum, 2004: Synoptic-scale precursors to significant cold-season precipitation events in Burlington, Vermont. *Wea. Forecasting,* **19,** 841–854.

Tibaldi, S., F. D'Andrea, E. Tosi, and E. Roeckner, 1997: Climatology of Northern Hemisphere blocking in the ECHAM model. *Climate Dyn.,* **13,** 649–666.

Trenberth, K. E., 1978: On the interpretation of the diagnostic quasi-geostrophic omega equation. *Mon. Wea. Rev.,* **106,** 131–137.

Uccellini, L. W., and P. J. Kocin, 1987: The interaction of jet streak circulations during heavy snow events along the east coast of the United States. *Wea. Forecasting,* **2,** 289–308.

Uppala, S. M., and Coauthors, 2005: The ERA-40 Re-Analysis. *Quart. J. Roy. Meteor. Soc.,* **131,** 2961–3012.

Walker, G. T., and E. W. Bliss, 1932: World Weather V. *Memo. J. Roy. Meteor. Soc.,* **4,** 53–84.

Wallace, J. M., and D. S. Gutzler, 1981: Teleconnections in the geopotential height field during the Northern Hemisphere winter. *Mon. Wea. Rev.,* **109,** 784–812.

Wernli, H., and H. C. Davies, 1997: A Lagrangian-based analysis of extratropical cyclones. I: The method and some applications. *Quart. J. Roy. Meteor. Soc.,* **123,** 467–489.

Wilks, D. S., 2006: *Statistical Methods in the Atmospheric Sciences*. 2nd ed. Academic Press, 627 pp.

Woollings, T., B. Hoskins, M. Blackburn, and P. Berrisford, 2008: A new Rossby wave–breaking interpretation of the North Atlantic Oscillation. *J. Atmos. Sci.,* **65,** 609–626.